Int. J. Electrochem. Sci., 15 **(2020)** 1128 – 1147, doi: 10.20964/2020.02.34

International Journal of
ELECTROCHEMICAL
SCIENCE
www.electrochemsci.org

Joint Estimation of Ternary Lithium-ion Battery State of Charge and State of Power Based on Dual Polarization Model

Yaqian Tan[1,2], Maji Luo[1,2,], Liyang She[1,2], and Xiangyu Cui[3]*

[1] Hubei Key Laboratory of Advanced Technology for Automotive Components, Wuhan University of Technology, Wuhan 430070, PR China
[2] Hubei Collaborative Innovation Center for Automotive Components Technology, Wuhan University of Technology, Wuhan 430070, PR China
[3] State Key Laboratory of Advanced Design and Manufacturing for Vehicle Body, Hunan University, Changsha, 410082, PR China
[*]E-mail: mjluo@whut.edu.cn

Received: 6 October 2019 / *Accepted:* 6 December 2019 / *Published:* 31 December 2019

The battery state of charge (SOC) and state of power capability (SOP) are the core elements of a battery management system (BMS) for ensuring efficient and safe driving in electric vehicles. In this paper, the SOC and the SOP are jointly estimated under multiple constraints by using the dual polarization (DP) model for a ternary lithium-ion battery, and the extended Kalman filter (EKF) algorithm has been used to improve the accuracy of state estimation and the calculational simplicity. The calculation equations for the multiple-constraint parameters are deduced. The power capability can be calculated rapidly based on the constraints on the current, voltage and SOC. The simulation and experimental results demonstrate that for both the SOC and the SOP, highly satisfactory prediction accuracy is realized under various operating conditions. The maximum SOP estimation error in the DP model is less than 2.1% for a battery with various SOC states, which corresponds to higher estimation accuracy than that of the Thevenin model. In addition, the SOP estimation model has strong robustness, which renders the joint estimation of the SOC and the SOP more reliable in the practical application of electric vehicles.

Keywords: Ternary lithium-ion battery, dual polarization model, extended Kalman filter, state of charge (SOC), state of power capability (SOP)

1. INTRODUCTION

The T-LiB (ternary lithium ion battery), as a promising solution to the exacerbation of fuel depletion and environmental disruption produced by traditional fuel vehicles, is an important vehicle energy storage device that has received extensive attention in the electric vehicle industry. To ensure safe, durable, and efficient driving performance of the battery under various operating conditions and

during interactions with charging piles, an excellent battery management system (BMS) is essential and has been devised to furnish estimation, monitoring, equalization, control and communication functions to improve the battery efficiency. Among these, accurate real-time state estimation within the battery is the key role of BMS. However, due to the formidable nonlinearity and time-variability, along with the inconsistency among battery packs, the reliable and accurate estimation of the state of charge (SOC) and the state of power capability (SOP) remains challenging [1-3].

A reliable prediction of the battery's states is based on an accurate battery model, which can represent the internal characteristics of the battery [4]. Many battery models have been presented, which include the neural network model, the electrochemical model [5], and equivalent circuit models (ECMs) [6]. The first two models are not suitable for practical applications in electric vehicles because they require complicated calculations and are unstable models. The equivalent-circuit models that use electric components to approximate the battery dynamics are the most widely used. The commonly used equivalent circuit models are the resistance model (Rint), the first-order resistor-capacitor (RC) model (Thevenin), the second-order RC model (DP) [7], and PNGV. In Ref. [8, 9], the second-order RC model has been applied to determine the state of charge, and satisfactory estimation accuracy was realized. In Ref. [10-12], the DP model performs the best in estimating the SOC with the extended Kalman filter (EKF) algorithm on the basis of three operating conditions. Nejad [13] obtained a similar conclusion by using FUDS, finding that the state estimation within the DP model has the highest precision. In Ref. [14], a comprehensive comparison of equivalent circuit models demonstrates that the maximum error of the DP model is much smaller than that of the Thevenin model. Considering both the model accuracy and the simplicity of the mathematical analysis, the DP model with two-RC hysteresis is adopted in this paper.

The SOC is critical for the energy management system of the battery, which refers to the remaining charge and is the basis of the charge and discharge control strategy and the system security [15]. It is the hidden state inside the battery and is determined via non-direct measurement. Therefore, accurate and rapid estimation of the battery SOC has become the main focus and challenge of the BMS [16]. For overcoming these difficulties, various approaches for estimation have been proposed, such as the ampere-hour integration method [17], genetic algorithms [18], the open-circuit voltage method [19], the particle filter (PF) [20], the neural network method [21], the grey extended Kalman filter [22], the extended Kalman filter (EKF) [23-25], and artificial intelligence [26]. In addition, adaptive filter techniques and observer methods [27-30] have been designed for determining the battery SOC rapidly. Ye [31] uses the improved adaptive particle swarm filter algorithm to estimate the SOC. Wei [32] proposes a multi-timescale approach with on-line battery parameter identification for simultaneously estimating the SOC and the battery capacity. Among these methods, the Kalman-filter-based approaches perform the best in practical applications, especially the EKF and the unscented Kalman filter (UKF) algorithms. Nevertheless, the UKF uses predetermined sampling points in the system sampling, which is a complicated calculation process. Thus, the EKF [33-35] is a useful approach for determining the SOC exactly, which is the research objective in this study, and the EKF is implemented via a simple algorithm. In addition, it can self-correct if a large error occurs in the estimation of the system, and its filtering theory can substantially reduce the impact of sampling noise. In Ref. [36], the EKF is integrated with the multi-model method and is used to estimate navigation information according to various error

models to provide an optimal estimate for the state. To improve the state estimation accuracy and to simplify the calculation process, this paper use the EKF to estimate the SOC.

For the estimation of the battery power usage in electric vehicles and the regulation of the propelling power of starting, speeding up, climbing, and regenerative braking, a reliable SOP estimation is of substantial importance. Nevertheless, the power capability cannot be measured by measuring equipment directly [37]. Ref. [38] describes a common method for measuring the power capability using the hybrid pulse power characterization (HPPC) test. This method considers only the battery voltage limit, which inevitably leads to reductions in the accuracy and adaptability. In addition, the employed Rint model cannot identify the dynamic characteristic of the battery. Therefore, it can be only used in the laboratory. Regarding the SOP estimation, various algorithms that are based on dynamic battery models are available for ensuring efficient and safe driving [39]. In Ref. [40, 41], the state of energy (SOE) is considered when estimating the SOP with multi-constrained conditions; however, the use of the Thevenin model reduces the algorithm accuracy by ignoring the model precision. In Ref. [42], the temperature effect is calculated in the SOP estimation of multi-parameter constraints. However, model-based SOP estimation with a RC circuit of a dynamic equivalent circuit model is not precise. Wei [43] presents an AF-RTLS technique combined with a Luenberger observer to compensate for noise interference by gaining control, and the SOP estimate is extracted by utilizing the first-order battery model without sufficient model accuracy. Other proposed SOP estimation methods are also based on the Thevenin model and ignore the dynamics characteristics inside the model [44]. Since the SOC and the SOP are mutually interactive, it is valuable to discuss the joint estimation of the SOC and the SOP under multi-parameter constraints. A critical result of this paper is the development of a multi-parameter joint estimation method for the state of charge and the state of power under the DP battery model. The DP model with two RC loop circuits is used to estimate the status parameter with higher model accuracy. The joint estimation for the SOC and the SOP is conducted on the basis of the EKF technique to improve the estimation accuracy and the calculational simplicity. Moreover, various conditions are used to evaluate the joint estimation performance, and the low-order equivalent circuits are compared in terms of estimation accuracy.

The paper is divided into four parts. Section 2 represents the employed equivalent-circuit model and parameter identification approach. Section 3 reviews the EKF algorithm on the basis of the DP model, and an approach for the multi-parameter-constraint joint estimation of the SOC and the SOP is developed. The proposed multi-parameter-constraint joint estimation method with various profiles is evaluated in Section 4. The conclusions of this study are summarized in the last part.

2. PROPOSED BATTERY MODEL AND PARAMETER IDENTIFICATION METHOD

2.1. Battery Model

The accuracy of state estimation and the calculational simplicity vary among battery models. Therefore, a reliable battery model must be established prior to obtaining a state estimate with high accuracy. In the practical BMS, the equivalent circuit model, which is based on the resistor and the

capacitor, is widely used [9, 45-47]. For this study, the DP model, which includes an open-circuit voltage, an ohmic resistance and two resistor-capacitor (*RC*) loop circuits, is used as the battery model, a schematic diagram of which is displayed in Fig. 1. The open-circuit voltage *(U_{OCV})* is a function of the SOC value. The ohmic resistance *(R_0)* of the battery mainly refers to the impedance that is caused by the material structure of the electrode and the connection resistance. Two RC networks with polarization resistances (R_{p1}, R_{p2}) and polarization capacitances (C_{p1}, C_{p2}) are used to simulate the dynamic electrochemical polarization and concentration polarization.

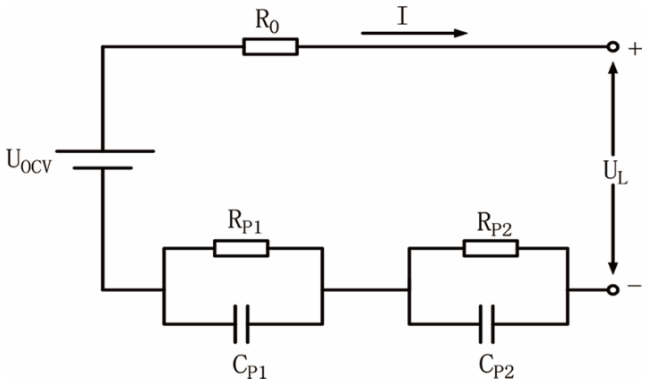

Figure 1. Schematic diagram of the equivalent circuit model

In Fig. 1, U_{P1}, U_{P2}, and U_L are the two polarization voltages that are generated by *RC* circuits and the terminal voltage, respectively, and I is the load current, where discharge is defined as positive. The electrical conduction of the battery model can be expressed by Equation (1).

$$\begin{cases} U_L = U_{ocv} - IR_0 - U_{P1} - U_{P2} \\ \dot{U_{P1}} = -\dfrac{1}{C_{P1}R_{P1}}U_{P1} + \dfrac{1}{C_{P1}}I \\ \dot{U_{P2}} = -\dfrac{1}{C_{P2}R_{P2}}U_{P2} + \dfrac{1}{C_{P2}}I \end{cases} \tag{1}$$

where $\dot{U_{P1}}$ and $\dot{U_{P2}}$ are the derivatives of U_{P1} and U_{P2}, respectively. The battery state equation in Equation (1) can be discretized as follows:

$$\begin{cases} U_L(k) = U_{ocv} - I_kR_0 - U_{P1}(k) - U_{P2}(k) \\ U_{P1}(k+1) = U_{P1}(k)e^{-\frac{T_S}{\tau_1}} + I_{k+1}R_{P1}(1 - e^{-\frac{T_S}{\tau_1}}) \\ U_{P2}(k+1) = U_{P2}(k)e^{-\frac{T_S}{\tau_2}} + I_{k+1}R_{P2}(1 - e^{-\frac{T_S}{\tau_2}}) \end{cases} \tag{2}$$

2.2. Parameter Identification Method

Prior to describing the dynamic characteristics of the battery, the model parameters must be identified reliably, which include U_{OCV}, R_0, R_P, and C_P. In this paper, nonlinear offline identification [9, 48] is used to obtain the parameters, which analyses the voltage response curve of the HPPC. Fig. 2 presents the battery terminal voltage and current changes that occur during an HPPC experiment at one SOC point.

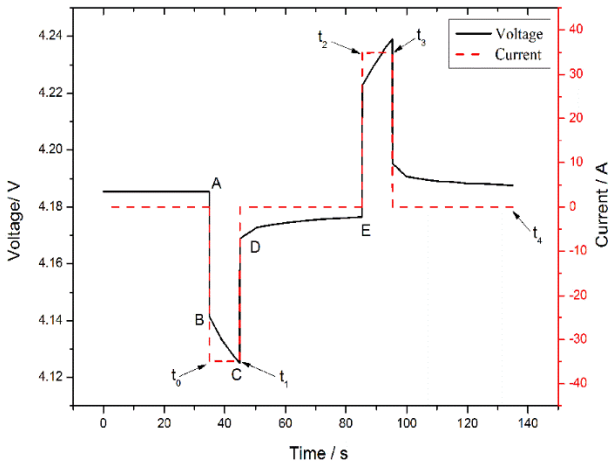

Figure 2. Curves of the HPPC test voltage and current response

The average value of the two terminal voltages after the charging and discharging processes is used as the open-circuit voltage U_{OCV} to reduce the effect of the rebound voltage.

Affected by ohmic resistance R_0, the terminal voltage changes rapidly with the change of the current from I to 0. For reducing noise interference to R_0, the charge-discharge resistances are calculated and the average value of voltage values of AB and CD is used to calculate R_0 by Equation (3).

$$R_0 = \frac{\Delta U_{AB} + \Delta U_{DC}}{2I} \tag{3}$$

During the period from t_2 to t_3, the terminal voltage changes slowly due to the polarization effect. Based on Equation (1), the terminal voltage $U_L(t)$ can be expressed as an exponential function, which is presented as Equation (4).

$$U_L(t) = U_{OCV} - U_1(0)e^{-t/\tau_1} - U_2(0)e^{-t/\tau_2} \tag{4}$$

Suppose $U_1(0) = b_1$ and$U_2(0) = b_2$. Then:

$$U_L(t) = U_{OCV} - b_1 e^{-t/\tau_1} - b_2 e^{-t/\tau_2} \tag{5}$$

From the measurement data of the terminal voltage, the values of b_1, b_2, τ_1 and τ_2 in the above equation can be acquired through exponential fitting with the cftool fitting toolbox in the MATLAB software.

τ_1 and τ_2 are the polarization time constants in the RC circuits of ECM, which can be expressed as:

$$\begin{cases} \tau_1 = C_{P1}R_{P1} \\ \tau_2 = C_{P2}R_{P2} \end{cases} \tag{6}$$

Since the polarization voltage cannot change in the process from point C to point D, the instantaneous voltages at the two points are equal. Thus, Equation (6) can be obtained.

$$\begin{cases} \{I \times R_{P1}(1 - e^{-t_c/\tau_1}) = b_1 \\ \{I \times R_{P2}(1 - e^{-t_c/\tau_2}) = b_2 \end{cases} \tag{7}$$

Comparing Equations (6) and (7), we obtain polarization parameters R_{P1}, C_{P1}, R_{P2}, and C_{P2}.

3. JOINT ESTIMATION APPROACH UNDER A MULTI-PARAMETER CONSTRAINT

3.1. State of Charge Estimation Based on EKF

In a linear system, Kalman filtering can be used to calculate the system state with the state equation according to the system input and output. Nonlinear systems, such as lithium-ion battery systems, require the use of the EKF algorithm to linearize the state-space equation with the Taylor formula, from which the second-order and higher order terms are omitted. The calculation procedure of the EKF arithmetic that is based on the time series that is defined in this paper is presented in Table 1.

The SOC refers to the ratio of the residual capacity to the capacity of the fully charged state. The traditional amperage integration method for estimating the SOC is based on Equations (8). Considering the negative effects of the suboptimal sensor precision, battery ageing and self-discharge on the SOC estimation performance, this paper combines the EKF algorithm with the traditional amperage integration method to estimate the SOC to realize the self-correction of the SOC.

$$SOC(t) = SOC(t_0) - \frac{\eta}{C_N}\int_{t_0}^{t} i(t)dt \tag{8}$$

where η is the coulomb efficiency, which is determined by the current, temperature, and capacity, and C_N is the capacity of the fully charged state, where C_N=35 Ah.

Table 1. Algorithm of the extended Kalman filter

The nonlinear state-space equation : $\begin{cases} x_{k+1} = f(x_k, u_k) + \omega_k \\ y_k = g(x_k, u_k) + v_k \end{cases}$

Linearization equation: $\begin{cases} x_{k+1} \approx f(\hat{x}_k, u_k) + \frac{\partial f}{\partial \hat{x}_k}(x_k - \hat{x}_k) + \omega_k \\ y_k \approx g(\hat{x}_k, u_k) + \frac{\partial g}{\partial \hat{x}_k}(x_k - \hat{x}_k) + v_k \end{cases}$

Suppose $\frac{\partial f}{\partial \hat{x}_k} = A_k$ and $\frac{\partial g}{\partial \hat{x}_k} = C_k$. Then,

$\begin{cases} x_{k+1} \approx A_k x_k + [f(\hat{x}_k, u_k) - A_k \hat{x}_k] + \omega_k \\ y_k \approx C_k x_k + [g(\hat{x}_k, u_k) - C_k \hat{x}_k] + v_k \end{cases}$

(1) Initialization:

$\hat{x}_{0/0} = E(x_0), P_{0/0} = var(x_0)$

(2) State estimate update:

$\hat{x}_{k/k-1} = f\left(\hat{x}_{k-1/k-1}, u_{k-1}\right) = A_{k-1}\hat{x}_{k-1/k-1} + B_{k-1}u_{k-1}$

Error covariance update:

$P_{k/k-1} = A_{k-1}P_{k-1/k-1}A_{k-1}^T + Q_k$

(3) Kalman gain matrix:

$L_k = P_{k/k-1}C_k^T\left[C_k P_{k/k-1}C_k^T + R_k\right]^{-1}$

(4) State estimate measurement update:

$\hat{x}_{k/k} = \hat{x}_{k/k-1} + L_k\left[y_k - g\left(\hat{x}_{k/k-1}, u_k\right)\right]$

Error covariance measurement update:

$P_{k/k} = (E - L_k C_k)P_{k/k-1}$

In these equations, x_k is the state variable at time k, u_k is the input variable, y_k is the observation variable, ω is the process noise, ν is the measured noise, and ω and ν are independent. $g(x_k, u_k)$ and $f(x_k, u_k)$are the observation function and the state function, respectively, of the system.

After discretization and linearization of Equations (2), the state and observation equations of the battery can be obtained via Equations (9) and (10)

$$\begin{bmatrix} U_{P1,k} \\ U_{P2,k} \\ SOC_k \end{bmatrix} = \begin{bmatrix} e^{-\frac{T_S}{\tau_1}} & 0 & 0 \\ 0 & e^{-\frac{T_S}{\tau_2}} & 0 \\ 0 & 0 & 1 \end{bmatrix} \begin{bmatrix} U_{P1,k-1} \\ U_{P2,k-1} \\ SOC_{k-1} \end{bmatrix} + \begin{bmatrix} R_{P1}(1 - e^{-\frac{T_S}{\tau_1}}) \\ R_{P2}(1 - e^{-\frac{T_S}{\tau_2}}) \\ \frac{\eta T_S}{C_N} \end{bmatrix} [i_{k-1}] + \begin{bmatrix} \omega_{1.k-1} \\ \omega_{2.k-1} \\ \omega_{3.k-1} \end{bmatrix} \tag{9}$$

$$[U_{L,k}] = [-1 \quad -1 \quad 0] \begin{bmatrix} U_{P1,k-1} \\ U_{P2,k-1} \\ SOC_{k-1} \end{bmatrix} - [R_0][i_k] + [U_{OCV}] + [\nu_k] \tag{10}$$

where $\omega_{1.k-1}, \omega_{2.k-1}$ and $\omega_{3.k-1}$ denote the noises of the three state variables and ν_k is the observation noise. Equation (11) presents the correlative SOC estimation matrices, which have been deduced from the state equation of the battery.

$$A_k = \begin{bmatrix} e^{-\frac{T_S}{\tau_1}} & 0 & 0 \\ 0 & e^{-\frac{T_S}{\tau_2}} & 0 \\ 0 & 0 & 1 \end{bmatrix}, B_k = \begin{bmatrix} R_{P1}(1 - e^{-\frac{T_S}{\tau_1}}) \\ R_{P2}(1 - e^{-\frac{T_S}{\tau_2}}) \\ \frac{\eta T_s}{C_N} \end{bmatrix} \tag{11}$$

$$C_k = \frac{\partial U_L}{\partial x_k} = \begin{bmatrix} \frac{\partial U_L}{\partial U_{P1}} & \frac{\partial U_L}{\partial U_{P2}} & \frac{\partial U_L}{\partial SOC} \end{bmatrix} \tag{12}$$

$$\frac{\partial U_L}{\partial U_{P1}} = -1, \frac{\partial U_L}{\partial U_{P2}} = -1, \frac{\partial U_L}{\partial SOC} = \frac{\partial U_{OCV}}{\partial SOC} - i \times \frac{\partial R_0}{\partial SOC} \tag{13}$$

U_{OCV} and the ohmic resistance are sixth-order polynomial functions of the SOC; hence, $\frac{\partial U_{OCV}}{\partial SOC}$ and $\frac{\partial R_0}{\partial SOC}$ can be obtained by partial differentiation based on Equations (14) and (15). For simplicity of expression, the SOC is replaced with *z*.

$$\frac{\partial U_{OCV}}{\partial SOC} = a_1 + 2a_2 z^1 + 3a_3 z^2 + 4a_4 z^3 + 5a_5 z^4 + 6a_6 z^5 \tag{14}$$

$$\frac{\partial R_0}{\partial SOC} = b_1 + 2b_2 z^1 + 3b_3 z^2 + 4b_4 z^3 + 5b_5 z^4 + 6b_6 z^5 \tag{15}$$

3.2. State of Power Capability Estimation

3.2.1. Estimation based on the Voltage Constraint

Automotive applications require continuous power capability estimates, and the current capability calculator should be constructed first. Assuming that the system input is unchanged from the *kth* sampling time t_k to the *(k+L)th* sampling time t_{k+L}, namely, $u_{k+L} = u_k$within the sampling intervals of $L*\triangle t$, the discrete state-space equation of the battery model at the discrete-time index *k* + *L* is

expressed by Equation (16). L is an integer that is determined by the actual energy demand of the vehicle. For example, hybrid electric vehicles require 10 s of continuous power to accelerate, climb or brake; thus, the value of L is defined as $10/\triangle t$. In this study, the value of L is set to 300, and the sampling interval is 0.1 s; hence, we require 30 s of continuous power capability.

$$\begin{cases} x_{k+L} = A_{k+L}x_{k+L-1} + B_{k+L}u_{k+L-1} \\ y_{k+L} = C_{k+L}x_{k+L} + D_{k+L} \end{cases} \tag{16}$$

The parameters of the battery change slowly and there are minimal differences with the model parameters of the adjacent SOC. Therefore, the battery model can be regarded as a model parameter constant system within 30-s duration of power:

$$x_{k+L} = A_k^L x_k + (\sum_{j=0}^{L-1} A_K^{L-1-j} x_k B_K) u_k \tag{17}$$

The peak power calculation is based on the DP model, and the terminal voltage and polarization voltage in a continuous period can be obtained from Equations (18) and (19).

$$U_{L,k+L} = U_{ocv}(z_{k+L}, C_N) - U_{P1,k+L} - U_{P2,k+L} - R_i i_{k+L} \tag{18}$$

$$\begin{aligned} U_{P,k+L} &= U_{P1,k+L} + U_{P2,k+L} \\ &= \left(e^{-\frac{T_S}{\tau_1}}\right)^L U_{P1,k} + i_{L,k}R_{P1}(1 - e^{-\frac{T_S}{\tau_1}}) \sum_{j=0}^{L-1} \left(e^{-\frac{T_S}{\tau_1}}\right)^{L-1-j} + \left(e^{-\frac{T_S}{\tau_2}}\right)^L U_{P2,k} \\ &+ i_{L,k}R_{P2}(1 - e^{-\frac{T_S}{\tau_2}}) \sum_{j=0}^{L-1} \left(e^{-\frac{T_S}{\tau_2}}\right)^{L-1-j} \end{aligned} \tag{19}$$

In addition, the SOC is a function of the current within the continuous sampling interval, and U_{OCV} depends on the SOC and the battery capacity. Thus, Equations (18) cannot be directly applied to the solution of the current capability. To decouple the nonlinear relation, the independent function $g\,(z, C_n)$ is used to define the $U_{OCV,}$ and the first-order Taylor expansion of U_{OCV} is used to obtain the current capability estimate with the high-order terms omitted, which is expressed as follows:

$$\begin{aligned} U_{ocv}(z_{k+L}, C_N) &= U_{ocv}\left(z_k - {\eta i_k L \times T_S}/{C_N}, C_N\right) \\ &\approx U_{ocv}(z_k, C_N) - i_k {\eta L \times T_S}/{C_N} \left.\frac{\partial U_{OCV}}{\partial z}\right|_{z=z_k} \end{aligned} \tag{20}$$

Then:

$$\begin{aligned} U_{L,k+L} = U_{ocv}(z_k, C_N) &- i_k {\eta L \times T_S}/{C_N} \left.\frac{\partial U_{OCV}}{\partial z}\right|_{z=z_k} \\ &- \left[\left(e^{-\frac{T_S}{\tau_1}}\right)^L U_{P1,k} + i_k R_{P1}(1 - e^{-\frac{T_S}{\tau_1}}) \sum_{j=0}^{L-1} \left(e^{-\frac{T_S}{\tau_1}}\right)^{L-1-j} + \left(e^{-\frac{T_S}{\tau_2}}\right)^L U_{P2,k} + i_k R_{P2}(1 \right. \\ &\left. - e^{-\frac{T_S}{\tau_2}}) \sum_{j=0}^{L-1} \left(e^{-\frac{T_S}{\tau_2}}\right)^{L-1-j}\right] - R_i i_k \end{aligned} \tag{21}$$

In the end, the current capability estimates that are based on the voltage constraint between t_k and t_{k+L} are expressed as:

$$\begin{cases} i_{max,k+L}^{dis,V} = \dfrac{U_{ocv}(z_k, C_N) - \left(e^{-\frac{T_S}{\tau_1}}\right)^L U_{P1,k} - \left(e^{-\frac{T_S}{\tau_2}}\right)^L U_{P2,k} - U_{L,min}}{L \times \eta T_S / C_N \left.\frac{\partial U_{OCV}}{\partial z}\right|_{z=z_k} + R_{P1}\left(1 - e^{-\frac{T_S}{\tau_1}}\right)\sum_{j=0}^{L-1}\left(e^{-\frac{T_S}{\tau_1}}\right)^{L-1-j} + R_{P2}\left(1 - e^{-\frac{T_S}{\tau_2}}\right)\sum_{j=0}^{L-1}\left(e^{-\frac{T_S}{\tau_2}}\right)^{L-1-j} + R_i} \\ i_{min,k+L}^{chg,V} = \dfrac{U_{ocv}(z_k, C_N) - \left(e^{-\frac{T_S}{\tau_1}}\right)^L U_{P1,k} - \left(e^{-\frac{T_S}{\tau_2}}\right)^L U_{P2,k} - U_{L,max}}{L \times \eta T_S / C_N \left.\frac{\partial U_{OCV}}{\partial z}\right|_{z=z_k} + R_{P1}\left(1 - e^{-\frac{T_S}{\tau_1}}\right)\sum_{j=0}^{L-1}\left(e^{-\frac{T_S}{\tau_1}}\right)^{L-1-j} + R_{P2}\left(1 - e^{-\frac{T_S}{\tau_2}}\right)\sum_{j=0}^{L-1}\left(e^{-\frac{T_S}{\tau_2}}\right)^{L-1-j} + R_i} \end{cases} \quad (22)$$

where $U_{L,max}$ and$U_{L,min}$are the upper and lower limits, respectively, of the cut-off voltage, which are specified by the manufacturer, and $i_{max,k+L}^{dis,V}$ and $i_{min,k+L}^{chg,V}$are the maximum continuous discharge current and the minimum continuous charge, respectively, under the voltage limits.

3.2.2. Estimation based on the SOC Constraint

To prevent over-charging and over-discharging and to guarantee the safe operation of the battery, the current capability must be controlled when the actual SOC approaches the design limits. After considering the SOC limit voltage from Equation (8), the SOC-based current calculation formula for consecutive L sampling intervals is expressed by Equation (23).

$$\begin{cases} i_{max,k+L}^{dis,z} = \dfrac{z_k - z_{min}}{L \times \eta T_S / C_N} \\ i_{min,k+L}^{chg,z} = \dfrac{z_k - z_{max}}{L \times \eta T_S / C_N} \end{cases} \quad (23)$$

where $i_{max,k+L}^{dis,z}$ and $i_{min,k+L}^{chg,z}$are the maximum continuous discharge current and the minimum continuous charge current, respectively, that are based on the SOC constraints.

3.2.3. SOP Estimation under the Multi-Parameter Constraint

After calculating the current capability design limits, the continuous current estimates under multi-parameter constraints are calculated as follows:

$$\begin{cases} i_{max}^{dis} = min\{i_{max}, i_{max,k+L}^{dis,V}, i_{max,k+L}^{dis,z}\} \\ i_{min}^{chg} = max\{i_{min}, i_{min,k+L}^{chg,V}, i_{min,k+L}^{chg,z}\} \end{cases} \quad (24)$$

where i_{min} and i_{max} are the design limits for the minimum charge current and the maximum discharge current, respectively, and i_{min}^{chg} and i_{max}^{dis} are the minimum charge current and the maximum discharge current under multi-parameter constraints.

Then, the continuous power capability estimate with all limits enforced is presented in Equation (25).

$$\begin{cases} P_{max}^{dis} = U_{L,k+L} i_{max,k+L}^{dis} \\ P_{min}^{chg} = U_{L,k+L} i_{min,k+L}^{chg} \end{cases} \quad (25)$$

where P_{min}^{chg} and $P_{max}^{dis}$are the minimum charge peak power and the maximum discharge peak power, respectively.

Substituting the terminal voltage calculation of Equation (21) into Equation (25) yields:

$$\begin{cases} P_{max}^{dis} = i_{max,k+L}^{dis}\left(\begin{array}{c} U_{ocv}(z_k,C_N)-\left(e^{-\frac{T_S}{\tau_1}}\right)^L U_{P1,k}-\left(e^{-\frac{T_S}{\tau_2}}\right)^L U_{P2,k} \\ -i_{max,k+L}^{dis}\left(\begin{array}{c} L\times\eta T_S/C_N \left.\frac{\partial U_{OCV}}{\partial z}\right|_{z=z_k}+R_{P1}\left(1-e^{-\frac{T_S}{\tau_1}}\right)\sum_{j=0}^{L-1}\left(e^{-\frac{T_S}{\tau_1}}\right)^{L-1-j} \\ +R_{P2}\left(1-e^{-\frac{T_S}{\tau_2}}\right)\sum_{j=0}^{L-1}\left(e^{-\frac{T_S}{\tau_2}}\right)^{L-1-j}+R_i \end{array}\right) \end{array}\right) \\ P_{min}^{chg} = i_{min,k+L}^{chg}\left(\begin{array}{c} U_{ocv}(z_k,C_N)-\left(e^{-\frac{T_S}{\tau_1}}\right)^L U_{P1,k}-\left(e^{-\frac{T_S}{\tau_2}}\right)^L U_{P2,k} \\ -i_{min,k+L}^{chg}\left(\begin{array}{c} L\times\eta T_S/C_N \left.\frac{\partial U_{OCV}}{\partial z}\right|_{z=z_k}+R_{P1}\left(1-e^{-\frac{T_S}{\tau_1}}\right)\sum_{j=0}^{L-1}\left(e^{-\frac{T_S}{\tau_1}}\right)^{L-1-j} \\ +R_{P2}\left(1-e^{-\frac{T_S}{\tau_2}}\right)\sum_{j=0}^{L-1}\left(e^{-\frac{T_S}{\tau_2}}\right)^{L-1-j}+R_i \end{array}\right) \end{array}\right) \end{cases} \quad (26)$$

3.3. Joint Estimation Method of the SOC and the SOP

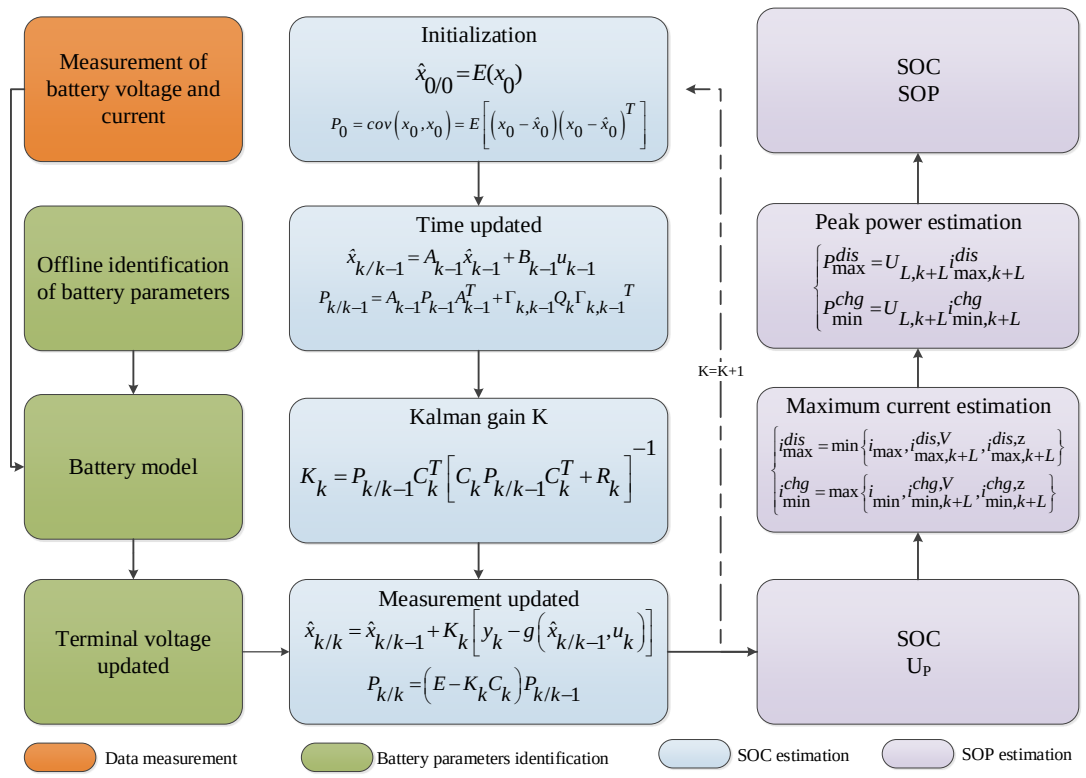

Figure 3. Flow diagram of the joint estimation method

From the above descriptions of the estimation algorithm, SOC and SOP interact with each other. Continuous power output leads to a rapid change in the SOC. Moreover, without a reliable power capability estimate, the SOC cannot be accurately obtained. Fig. 3 presents a flow diagram of the joint

estimation method, which includes onboard data measurement, offline parameter identification, SOC estimation, and SOP estimation.

4. RESULTS AND ANALYSIS

To evaluate the performance of the proposed joint estimation method, a simulation is designed. The test bench is introduced in Section 4.1. The SOC estimation performance is evaluated in Section 4.2. Section 4.3 presents the evaluations of the SOP.

4.1. Experimental Setup

The battery test platform of this study includes a high- and low-temperature alternating heat and humidity test chamber (GDJS-150), a PC controller, and a battery test system (Xinwei BTS-5V300A). The battery test system has multiple charge and discharge control modes, which can collect and store test data in real time. Its data acquisition step is up to 0.1 s, with ±0.3 A current control accuracy and ±0.005 V voltage control accuracy. The temperature test chamber can be used to simulate the battery temperature environment accurately with a temperature deviation of only 0.2 °C and a test temperature range of -50°C to 150°C. During the experiments, the battery is put in a test chamber for temperature control while connecting to the battery test system. This study chooses a commercial ternary material lithium-ion battery as the test object, which has an energy density of 160 wh/kg and a high-voltage platform; thus, it is easy to realize the accurate estimation of SOC. The performance parameters of the battery are listed in Table 2.

Table 2. Performance parameters of the battery

Items	Parameter values
Cathode materials	$LiNi_{1/3}Co_{1/3}Mn_{1/3}O_2$
Nominal capacity (Ah)	35
Nominal voltage (V)	3.7
Maximum continuous discharge current (C)	3
Maximum pulse discharge current (C)	5 (30 s)
Upper/lower cut-off voltage (V)	4.2/2.5

4.2. Performance of SOC Estimation

Through the algorithm that is proposed above, we can estimate the SOC for each sampling interval. For evaluating the accuracy of SOC estimation by EKF technology, three operating conditions

of T-LiB cells are used to conduct the evaluation: a constant-current discharge (CCD), HPPC and dynamic stress test (DST) conditions.

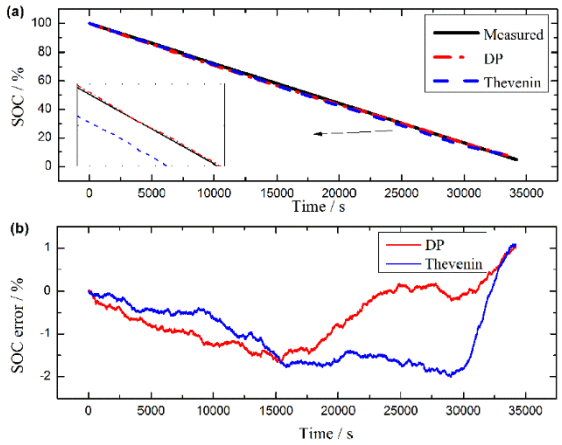

Figure 4. Comparison of SOC estimates between the DP and Thevenin models with CCD: (a) the SOC ; (b) the SOC error

The SOC estimates with CCD are presented in Fig. 4. The CCD condition is a static and stable condition, and the model accuracy can be evaluated based on the model estimation performance under the static condition. Fig. 4(a) presents the SOC comparison curve among the estimates of the DP and Thevenin models and the experimental measurement, while the estimated SOC error is plotted in Fig. 4(b). The results demonstrate that the estimated SOC error of the Thevenin model is less than 3%, while the maximum SOC estimation error of the EKF algorithm that is based on the DP model in the full-charge state range is less than 2%; hence, the proposed estimation method realizes satisfactory static estimation performance for the ternary lithium battery.

The SOC estimates in HPPC are presented in Fig. 5. The HPPC condition can be used not only for parameter identification, as a dynamic condition, but also to assess the estimation performance of the model. Fig. 5(a) presents the SOC comparison curve among the estimates of the DP and Thevenin models and the experimental measurement, while the estimated SOC error is plotted in Fig. 5(b). Twenty cycles are used to estimate the HPPC operating conditions. A static process lasts for an hour in each HPPC cycle; hence, the SOC will exhibit a stable state, which is the same as the estimation results in the diagram. From the estimation accuracy of the low-order equivalent model, the estimated values of the two models are close to the experimental values, and there is no abnormal alteration of the SOC; however, according to the enlarged diagram of (a), the estimation result of the DP model has more advantages. Combined with Fig. 5(b), the maximum error of estimating the SOC of the low-order equivalent circuit model does not exceed 3%; however, the maximum error of the DP model is smaller than that of the Thevenin model.

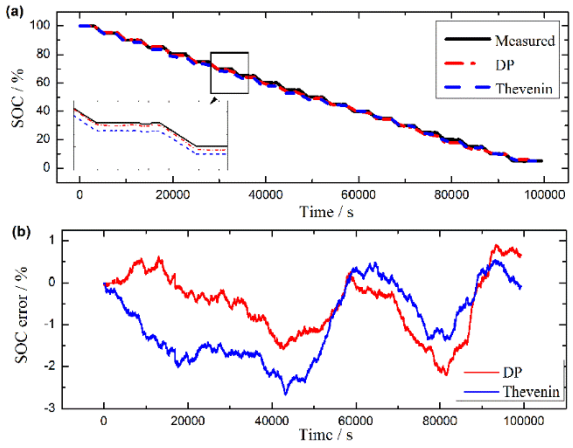

Figure 5. Comparison of the SOC estimates between the DP and Thevenin models in HPPC: (a) SOC; (b) SOC error

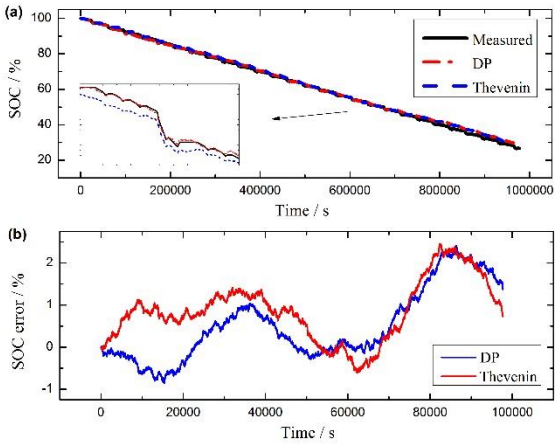

Figure 6. Comparison of the SOC estimates between the DP and Thevenin models in DST: (a) SOC; (b) SOC error.

The SOC estimates in DST are presented in Fig. 6. DST is a dynamic working condition, which can simulate the performance of a power cell with variable power, similar to HPPC. However, the frequency and amplitude of the current change are more complicated due to the simulation of the characteristics of starting, acceleration, uniform speed, braking, and climbing, among other actions. Fig. 6(a) presents the SOC comparison curve among the estimates of the DP and Thevenin models and the experimental measurement, while the estimated SOC error is plotted in Fig. 6(b). Comparing the simulation results with (a), the estimated curve of the model is highly coincident with the curve of the test. The variation of the current under the DST condition is more complex than that under the HPPC condition, which causes the estimation models to have larger prediction errors at both extremes of estimation, and it is difficult to track the true value. However, according to Fig. 6(b), the maximum estimated error of the SOC is still controlled within 2.5% under the more complicated variable-current conditions. This demonstrates that the estimation models realize satisfactory SOC estimation performance, and the DP model has lower error in the early stage of DST.

Table 3. Error analysis of SOC estimation

Condition	Model	Maximum error	Average error	Standard deviation
CCD	Thevenin	0.0201	0.0102	0.0073
	DP	0.0168	0.0059	0.0065
HPPC	Thevenin	0.0267	0.0097	0.0086
	DP	0.0223	0.0050	0.0073
DST	Thevenin	0.0246	0.0087	0.0096
	DP	0.0242	0.0051	0.0085

The mathematical statistical results of the SOC estimation error are presented in Table 3: under three working conditions, the maximum errors of SOC estimation in the DP model and the Thevenin model are less than 3%. However, the maximum error and the average error of the DP model are approximately 2% and 0.5%, respectively, which are smaller than those of the Thevenin model under static and dynamic conditions. Compared with the ESP-model-based EKF algorithm [49], the DP model yields a lower maximum SOC estimation error than 3.19%. According to reference [41], with the Thevenin-model-based UKF algorithm, the RMSE and MAE of SOC estimation under dynamic profiles are 0.0257 and 0.0207, respectively. In addition, the SOC estimation error of the PNGV-model-based UKF algorithm [50] is within 6%. In summary, the SOC estimation performance of the DP-model-based EKF algorithm is superior.

A reliable SOC estimate requires not only accurate estimation performance but also excellent robustness. It can be quickly corrected and converged to accurate values under inaccurate initial SOC values and various operating conditions.

Fig. 7 presents the results of the robustness analysis of the estimated SOC during discharge. The initial SOC of the discharge is 1 in the test, while the simulation process sets the initial SOC as 0.8. The simulation results demonstrate that when the SOC has an initial error at the beginning of discharge but converges to the real value quickly, the SOC can guarantee higher estimation accuracy; hence, the algorithm is robust.

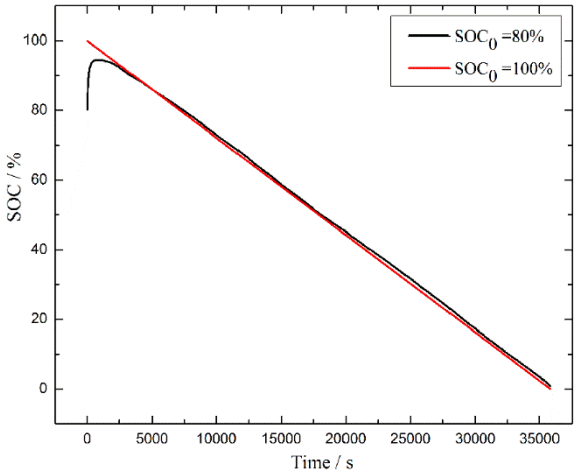

Figure 7. Robustness analysis of SOC estimation in the discharge process

4.3. Performance of SOP Estimation

For assessing the multi-parameter-constraint SOP estimation method, the SOC constraints of the T-LiB cells should be set, which vary among control strategies. The battery manufacturers set the voltage and current limits. Table 4 specifies a series of parameter limits of SOP estimation.

Table 4. Parameter limits of SOP estimation

Parameters	Maximum value	Minimum value
I (I_{max}, I_{min}) (A)	175	-105
U_L ($U_{L,max}$, $U_{L,min}$) (V)	4.2	2.5
SOC (SOC_{max}, SOC_{min}) (%)	90	10

Fig. 8 presents the estimated current capability and Fig. 9 presents the estimated power capability with an initial SOC of 100%. According to Fig. 8, the voltage, current and SOC constraints have important effects on the estimation of the maximum discharge current. In the first and middle periods of the discharge, the current constraint is effective, and the voltage constraint affects the peak current in the middle and late stages of the discharge. At the end, the current capability depends on the SOC constraint. If the peak power is always estimated under the same constraint condition, the estimated current value will be too large, and over-discharge of the battery will easily occur in the later stage of discharge, which will lead to irreversible and severe harm to the battery. Consequently, with the joint estimation of the SOC and the SOP within multi-parameter constraints, the battery can be used to avoid possible safety issues such as overcharge and over-discharge.

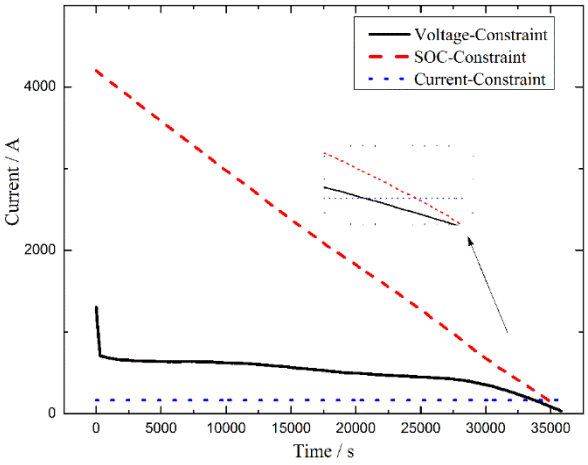

Figure 8. Maximum current variation curve with multi-parameter constraints

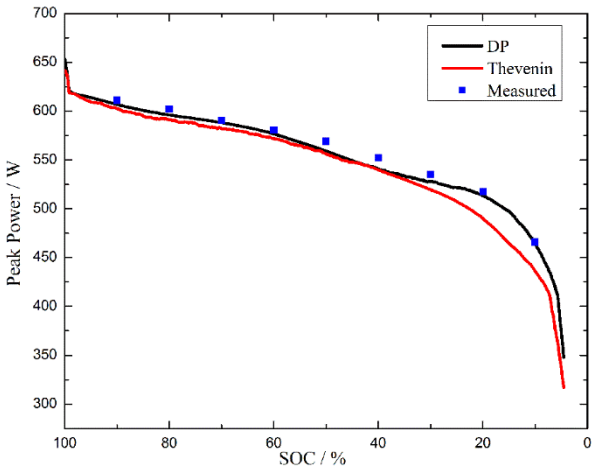

Figure 9. SOP estimation results in discharge

Fig. 9 compares the simulation and test results regarding the peak discharge power, in which the test data come from the results of 9 PPTs (peak power tests) in the range of 0.1-0.9 with an SOC interval of 0.1 using the USABC standard [38]. The simulation results of two types of low-order models are described as follows: the multi-state constrained SOP estimate of the equivalent circuit model is lower than the PPT experimental value, which is consistent with the results that were derived from the previous formulas. The simulation results of the DP model are closer to the experimental values, and the accuracy of SOP estimation is higher at the end of discharge than that of the Thevenin model. For the Thevenin model, the accuracy of SOP estimation is satisfactory at the initial stage but decreases substantially in the later stage of discharge. This decrease is observed because the battery parameters change with the increase of the temperature during the high-power discharge of the battery; hence, it is difficult for a single RC loop to accurately simulate the polarization effect.

Table 5. Analysis of Peak power

SOC	Tested power (W)	Estimation power (W)		Estimation error (%)	
		DP	Thevenin	DP	Thevenin
0.9	610.99	606.66	602.25	0.70	1.43
0.8	601.96	596.01	592.08	0.98	1.64
0.7	590.46	588.13	582.35	0.39	1.37
0.6	580.16	576.49	572.92	0.63	1.24
0.5	568.96	558.95	555.96	1.75	2.28
0.4	552.01	540.58	539.73	2.07	2.22
0.3	535.09	528.08	519.36	1.31	2.94
0.2	517.59	513.32	489.89	0.82	5.35
0.1	465.69	463.78	435.89	0.40	6.39

Table 5 is obtained by selecting the data of peak power within the SOC range of 0.1-0.9. The SOP estimation error of the Thevenin model increases with the decrease of the SOC up to 6.4%.

However, the maximum error and MAE of SOP estimation in the DP model are 2.1% and 0.469%, respectively, which can effectively avoid overcharging and over-discharging and fully realize the power performance of the battery. In reference [51], a 10-s power projection that is based on the adaptive and direct solution of the governing differential equations shows a deviation of 2.5%. The SOP that is estimated under multiple constraints based on DEKF [52] has a maximum relative error of 4%. Adding moving average (MA) noise to the Thevenin model [53], an SOP long-term discharge error of 2.72% is realized.

However, due to the differences in the requirements for the applications of peak power among electric vehicles, hybrid electric vehicles and fuel cell electric vehicles, the estimation performances of the power capability at various output times must be studied. Fig. 10 shows the peak power curve for the continuous power that is required for 1 s, 10 s, and 30 s during discharge. The power capability estimate decreases as the duration increases. Thus, the peak power and duration should be set to suitable values to protect the battery from safety damage.

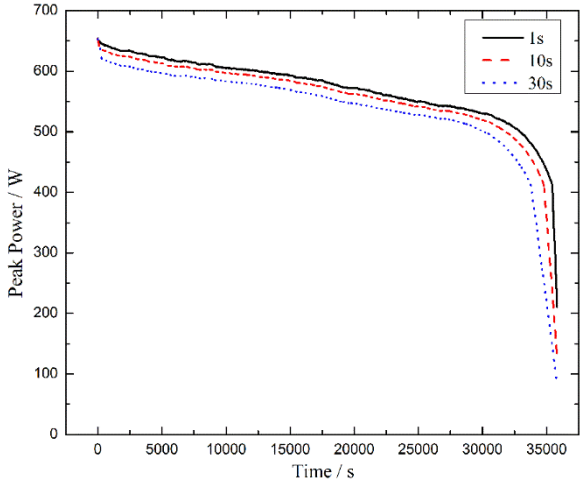

Figure 10. Power capability estimates for various durations

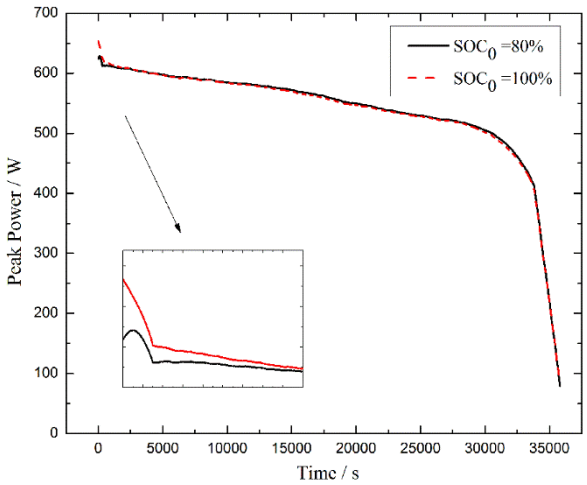

Figure 11. Robustness analysis of power capability estimation

The robustness analysis results of the power capability estimation method are presented in Fig. 11. The estimation profile of erroneous initial SOC has converged to the correct trajectory quickly, which demonstrates that the estimation method is highly robust.

Based on the above analysis, the proposed joint estimation of SOC and SOP with multi-parameter constraints performs well in estimating the SOC and the power capability. In addition, it can overcome an inaccurate initial SOC and has high robustness.

5. CONCLUSIONS

To obtain accurate SOC and power capability estimates in real time, the joint estimation of the SOC and SOP under multi-parameter constraints via the EKF algorithm has been proposed in this study. Through the real-time measurement and updating of the battery current and voltage, the battery parameters are accurately identified by an off-line fitting method to guarantee a reliable battery state estimate. The second-order RC model (DP) is used to reflect the dynamics of a ternary lithium-ion battery. Further, the model accuracy has been considered, along with the simplicity of calculation. Next, under the interrelationship of SOC and SOP, the EKF-based state observer is used for SOC estimation, and the SOP can be exactly calculated within the constraints of the current, voltage and SOC, which has high estimation accuracy and calculation simplicity. Finally, various operating conditions and robustness analysis of the battery are conducted to evaluate the performance of the proposed joint estimation approach. The results indicate the necessity of joint estimation under multi-parameter constraints and the robustness and high precision of the proposed method. Moreover, the error of estimation that is based on the DP model is smaller than that based on the Thevenin model, with a maximum error of less than 2.1%. As a result, the SOC and SOP joint estimates are reliable for practical application to electric vehicles. Our future work will revolve around the joint estimation of the battery state of health, the SOC and the SOP while considering the effect of single-cell inconsistency among batteries.

ACKNOWLEDGEMENT
This research was supported by the 111 project (Grant No. B17034).

References

1. Y. Zheng, M. Ouyang, X. Li, L. Lu, J. Li, L. Zhou and Z. Zhang, *Appl. Energy,* 183 (2016) 380.
2. M. A. Hannan, M. S. H. Lipu, A. Hussain and A. Mohamed, *Renewable & Sustainable Energy Reviews,* 78 (2017) 834.
3. S. Wang, L. Shang, Z. Li, H. Deng and Y. Ma, *Int. J. Electrochem. Sci.*, 10 (2015) 5130.
4. C. Lin, H. Mu, R. Xiong and W. Shen, *Appl. Energy,* 166 (2016) 76.
5. L. Zheng, L. Zhang, J. Zhu, G. Wang and J. Jiang, *Appl. Energy,* 180 (2016) 424.
6. F. Sun, R. Xiong, H. He, W. Li and J.E. E. Aussems, *Appl. Energy,* 96 (2012) 378.
7. S. Sepasi, R. Ghorbani and B.Y. Liaw, *J. Power Sources,* 245 (2014) 337.
8. B. Xia, W. Zheng, R. Zhang, Z. Lao and Z. Sun, *Energies*, 10 (2017).

9. B. Xia, Z. Sun, R. Zhang and Z. Lao, *Energies,* 10 (2017).
10. R. Xiong, J.Y. Cao, Q.Q. Yu, H.W. He and F.C. Sun, *IEEE Access,* 6 (2018) 1832.
11. X. Hu, S. Li and H. Peng, *J. Power Sources,* 198 (2012) 359.
12. Q. Wang, J. Wang, P. Zhao, J. Kang, F. Yan and C. Du, *Electrochimica Acta,* 228 (2017) 146.
13. S. Nejad, D.T. Gladwin and D.A. Stone, *J. Power Sources,* 316 (2016) 183.
14. L. Zhang, H. Peng, Z. Ning, Z. Mu and C. Sun, *Applied Sciences-Basel,* 7 (2017).
15. M. Luo, Y. Guo, J. Kang, L. She and Z. Geng, *Ionics,* 24 (2018) 1907.
16. Y. Guo, M. Luo, J. Zou, Y. Liu and J. Kang. *SAE International*, 2016.
17. H. Zhang, L. Zhao and Y. Chen, *Energies,* 8 (2015) 13811.
18. L. Chen, Z. Wang, Z. Lu, J. Li, B. Ji, H. Wei and H. Pan, *IEEE Trans. Power Electron.,* 33 (2018) 8797.
19. S. Lee, J. Kim, J. Lee and B.H. Cho, *J. Power Sources*, 185 (2008) 1367.
20. A. Tulsyan, Y. Tsai, R.B. Gopaluni and R.D. Braatz, *J. Power Sources,* 331 (2016) 208.
21. B. Xia, D. Cui, Z. Sun, Z. Lao, R. Zhang, W. Wang, W. Sun, Y. Lai and M. Wang, *Energy,* 153 (2018) 694.
22. H. Pan, Z. Lu, W. Lin, J. Li and L. Chen, *Energy,* 138 (2017) 764.
23. L. Zheng, J. Zhu, G. Wang, D.D.C. Lu and T. He, *Energy,* 158 (2018) 1028.
24. F. Claude, M. Becherif and H.S. Ramadan, *Int. J. Hydrogen Energy,* 42 (2017) 25509.
25. F. Yan, C. Zhang, C. Du and C.H. Cheng, *Int. J. Electrochem. Sci.,* 13 (2018) 12360.
26. A.G. Kashkooli, H. Fathiannasab, Z. Mao and Z. Chen, *J. Electrochem. Soc.,* 166 (2019) A605.
27. Z. Wei, C. Zou, F. Leng, B.H. Soong and K.J. Tseng, *IEEE Trans. Ind. Electron.,* 65 (2018) 1336.
28. C. Zou, X. Hu, S. Dey, L. Zhang and X. Tang, *IEEE Trans. Ind. Electron.,* 65 (2018) 5951.
29. X. Cui, Z. Jing, M. Luo, Y. Guo and H. Qiao, *Energies,* 11 (2018).
30. C. Zou, C. Manzie, D. Nesic and A.G. Kallapur, *J. Power Sources,* 335 (2016) 121.
31. M. Ye, H. Guo and B. Cao, *Appl. Energy,* 190 (2017) 740.
32. Z. Wei, J. Zhao, D. Ji and K.J. Tseng, *Appl. Energy,* 204 (2017) 1264.
33. Y. Ma, Q. Bai, L. Liang and H. Chen, *Proceedings of the 31st Chinese Control Conference*, Hefei ,China, 2012, 6815-6819.
34. C.S. Chin, Z. Gao, J.H. K. Chiew and C. Zhang, *Energies,* 11 (2018).
35. J. Sturm, H. Ennifar, S.V. Erhard, A. Rheinfeld, S. Kosch and A. Jossen, *Appl. Energy,* 223 (2018) 103.
36. H. Huang, X. Chen, B. Zhang and J. Wang, *ISA Trans.,* 66 (2017) 414.
37. C. Zou, A. Klintberg, Z. Wei, B. Fridholm, T. Wik and B. Egardt, *J. Power Sources,* 396 (2018) 580.
38. T.Q. Duong, *J. Power Sources,* 89 (2000) 244.
39. G.L. Plett, *IEEE Trans. Veh. Technol.,* 53 (2004) 1586.
40. X. Zhang, Y. Wang, J. Wu and Z. Chen, *Appl. Energy,* 216 (2018) 442.
41. Y. Wang, R. Pan, C. Liu, Z. Chen and Q. Ling, *J. Power Sources,* 374 (2018) 12.
42. W. Jiang, N. Zhang, P. Li and N. Chen, *Transbaltica 2017: Transportation Science and Technology*, Vilnius, Lithuania, 2017, 249-256.
43. Z. Wei, J. Zhao, R. Xiong, G. Dong, J. Pou and K.J. Tseng, *IEEE Trans. Ind. Electron.,* 66 (2019) 5724.
44. R. Xiong, F. Sun, H. He and N. Trong Duy, *Energy,* 63 (2013) 295.
45. Y.J. Zheng, W.K. Gao, M.G. Ouyang, L.G. Lu, L. Zhou and X.B. Han, *J. Power Sources,* 383 (2018) 50.
46. P. Shen, M.G. Ouyang, L.G. Lu, J.Q. Li and X.N. Feng, *IEEE Trans. Veh. Technol.,* 67 (2018) 92.
47. M. Cacciato, G. Nobile, G. Scarcella and G. Scelba, *IEEE Trans. Power Electron.,* 32 (2017) 794.
48. T. Wang, S. Chen, H. Ren and Y. Zhao, *Int. J. Energy Res.,* 42 (2018) 1603.
49. C. Yuan, B. Wang, H. Zhang, C. Long and H. Li, *Int. J. Electrochem. Sci.,* 13 (2018) 1131.

50. W. Wang, X. Wang, C. Xiang, C. Wei and Y. Zhao, *Ieee Access*, 6 (2018) 35957.
51. S. Wang, M. Verbrugge, J.S. Wang and P. Liu, *J. Power Sources*, 196 (2011) 8735.
52. S. Xiang, G. Hu, R. Huang, F. Guo and P. Zhou, Energies, 11 (2018).
53. T. Feng, L. Yang, X. Zhao, H. Zhang and J. Qiang, *J. Power Sources*, 281 (2015) 192.